Electronic Supplementary Material (ESI) for Physical Chemistry Chemical Physics.

Electronic Supplementary Information

Photolytic splitting of homodimeric quinone-derived oxetanes studied by ultrafast transient absorption spectroscopy and quantum chemistry

Alejandro Blasco-Brusola, Lorena Tamarit, Miriam Navarrete-Miguel, Daniel Roca-Sanjuán, Miguel A. Miranda, Ignacio Vayá

Table of contents

Fig. S11 A) LFP transient absorption spectra for NQ at different times after the laser pulse (0.5, 2, 5 and 20 μs). B) Decay traces for NQ (black) and NQ-Ox (blue) at 370 nm. All measurements were performed in deaerated MeCN at λ_{exc} = 266 nm.

Fig. S12 Degree of photodegradation for NQ (black) and NQ-Ox (blue) upon steady-state irradiation in deaerated MeCN using a multilamp photoreactor emitting at λ_{max} ~ 310 nm.

Fig. S13 Natural orbitals of the CASSCF active space of the singlet states at the oxetane structure for NQ-Ox.

Fig. S14 Natural orbitals of the CASSCF active space of the triplet states at the oxetane structure for NQ-Ox.

Fig. S15 Natural orbitals of the CASSCF active space of the singlet and triplet states at the diradical structure (^{3}NQ-Ox*) for NQ-Ox.

Fig. S16 Natural orbitals of the CASSCF active space of the singlet states at the crossing point structure (CP) for NQ-Ox.

Fig. S17 Natural orbitals of the CASSCF active space of the triplet states at the crossing point structure (CP) for NQ-Ox.

Fig. S18 Natural orbitals of the CASSCF active space of the singlet states at the transition state structure (TS) for NQ-Ox.

Fig. S19 Natural orbitals of the CASSCF active space of the triplet states at the transition state structure (TS) for NQ-Ox.

Fig. S20 Natural orbitals of the CASSCF active space of the singlet and triplet states at the excimer structure (^{3}EXC*) for NQ-Ox.

Fig. S21 T-shape and parallel conformations of the ^{3}EXC* for BQ-Ox system.

Fig. S22 T-shape and parallel conformations of the ^{3}EXC* for NQ-Ox system.

Table S1 Nature of the states in each relevant geometry for BQ-Ox: energies (E_v^{abs}; in eV), weight of the main configuration state functions in the CASSCF wavefunction and dipole moment (μ; in Debye). See shape of the natural orbitals in Figs. S4 to S9.

Table S2 Nature of the states in each relevant geometry for NQ-Ox: energies (E_v^{abs}; in eV), weight of the main configuration state functions in the CASSCF wavefunction and dipole moment (μ; in Debye). See shape of the natural orbitals in Figs. S11 to S18.

Table S3 DFT and CASPT2 energies of the T_1 state of both types of excimers of BQ-Ox and NQ-Ox. The energies are relative to their respective T-shape excimers.

Computational details

The calculations of this work were performed by means of Density Functional Theory (DFT) and multiconfigurational quantum chemistry (CASSCF[1] and CASPT2[2]) methods, using GAUSSIAN 09, revision D.01,[3] and MOLCAS 8[4] software packages, respectively.

Geometry optimizations. The structures of the singlet ground state of the oxetanes (BQ-Ox/NQ-Ox), the triplet state of the diradical (^{3}BQ-Ox*/^{3}NQ-Ox*), the triplet state of the exciplex (^{3}EXC*), the triplet transition state (TS) between the diradical and the exciplex and the isolated BQ molecules were optimized using the DFT method with the M06-2X functional, without any symmetry restriction and the standard 6-31++G** basis set.

On the one hand, a series of intermediate geometries between BQ-Ox/NQ-Ox and ^{3}BQ-Ox*/^{3}NQ-Ox* were obtained by scanning the C-C bond length. On the other hand, the intermediate geometries between ^{3}BQ-Ox*/^{3}NQ-Ox*, TS and ^{3}EXC* were determined by means of internal reaction coordinate calculations (IRC) from the TS. All of them were obtained with the DFT method and M06-2X/6-31++G** level of theory.

Excited-state single-point calculations. The ground- and excited-state energies on top of the optimized and scanned geometries were calculated using the state specific (SS)-CASPT2 method, which incorporates dynamic correlation, making use of the state averaged (SA)-CASSCF wave functions. In the case of BQ-Ox system, the active space used in the study was of 14 electrons distributed in 12 orbitals, demanding four singlet and four triplet states in the SA-CASSCF procedure and with the ANO-S-VDZP basis set, as implemented in MOLCAS 8 software package. For NQ-Ox, the active space was 12 electrons distributed in 12 orbitals and, in this case, three singlet and three triplet states were demanded. To ensure accuracy, the ionization-potential electron-affinity parameter[5] (IPEA) was set at 0.0 au in both systems. To minimize the presence of weakly intruder states, an imaginary level shift[6] of 0.2 au was applied.

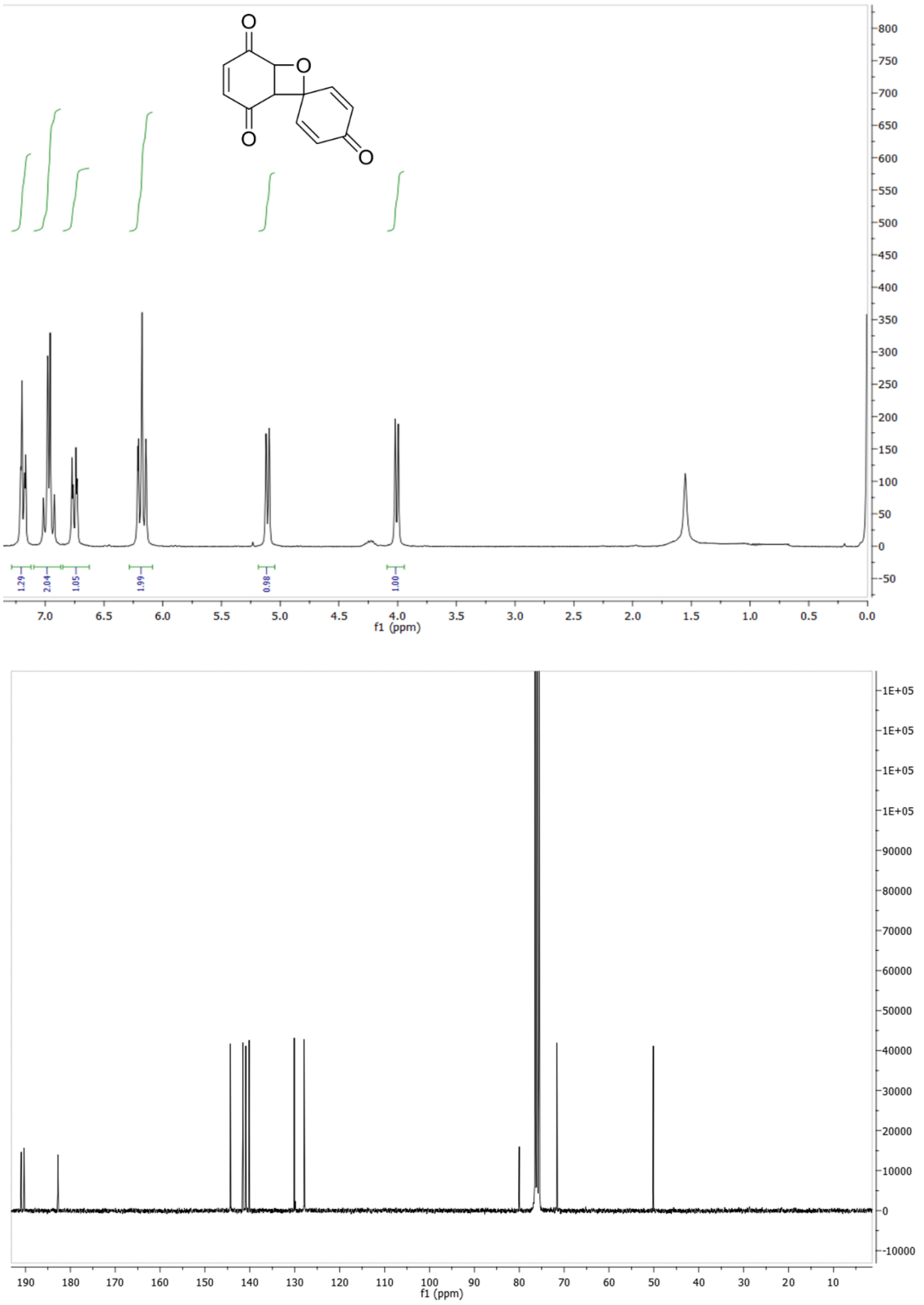

Fig. S1 ^{1}H- and ^{13}C-NMR for BQ-Ox in $CDCl_3$.

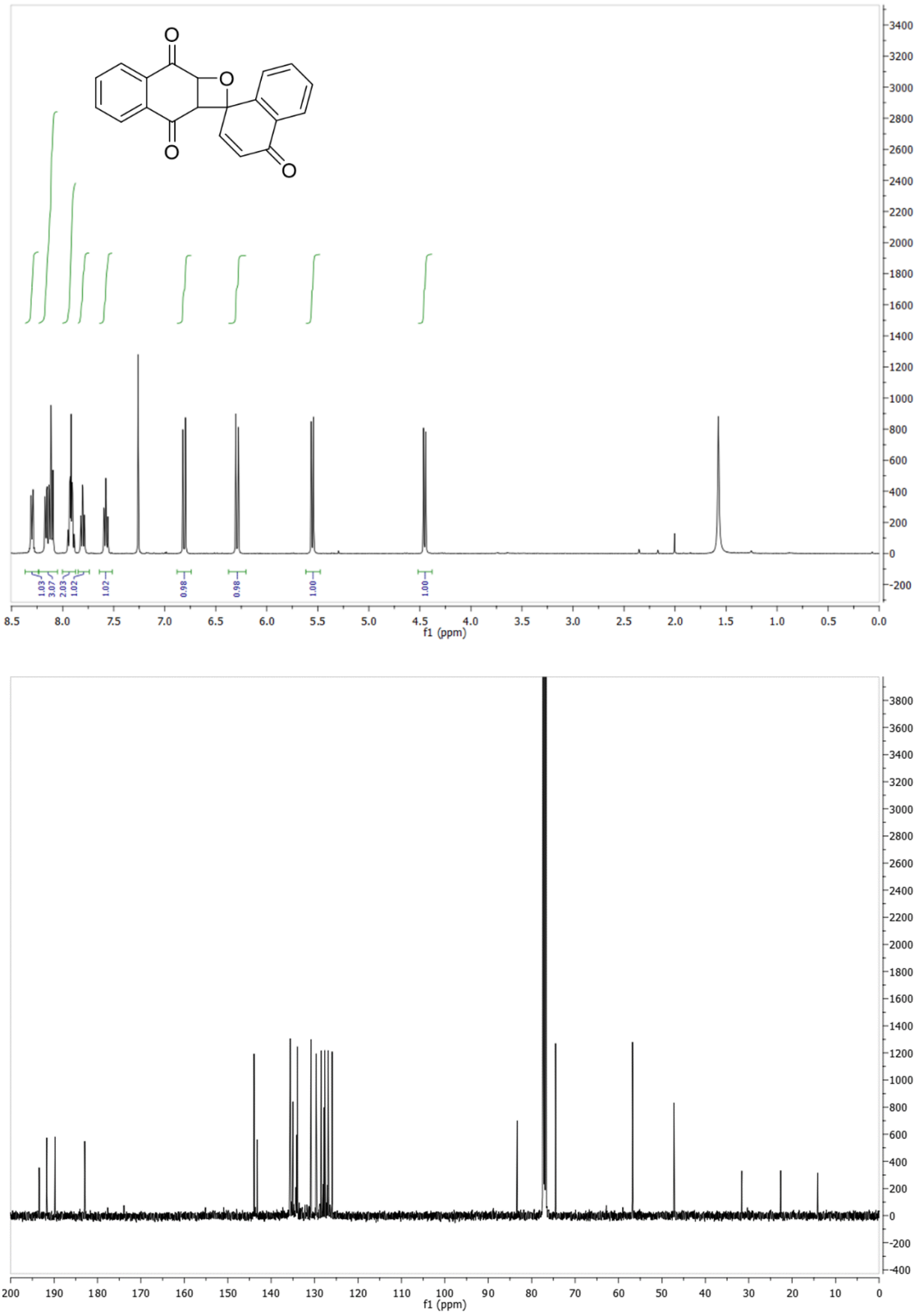

Fig. S2 ^{1}H- and ^{13}C-NMR for NQ-Ox in $CDCl_3$.

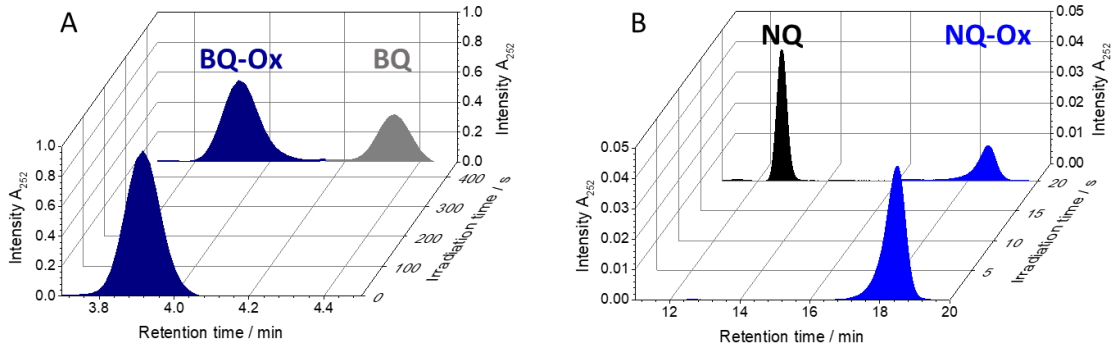

Fig. S3 Chromatograms of non-irradiated and irradiated BQ-Ox (A) and NQ-Ox (B) followed by analytical HPLC using a Photodiode Array Detector (wavelength fixed at 252 nm). Irradiations were performed in deaerated MeCN in a multilamp photoreactor emitting at λ_{max} ~ 310 nm through quartz cells.

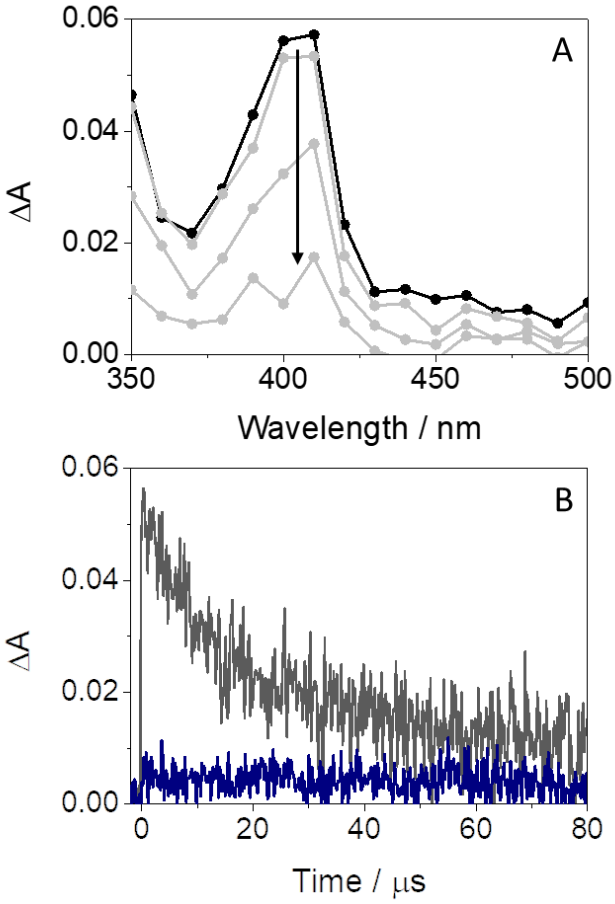

Fig. S4 LFP transient absorption spectra for BQ at different times after the laser pulse (1, 2, 10 and 50 μs). B) Decay traces for BQ (gray) and BQ-Ox (dark blue) at 410 nm. All measurements were performed in deaerated MeCN at λ_{exc} = 266 nm.

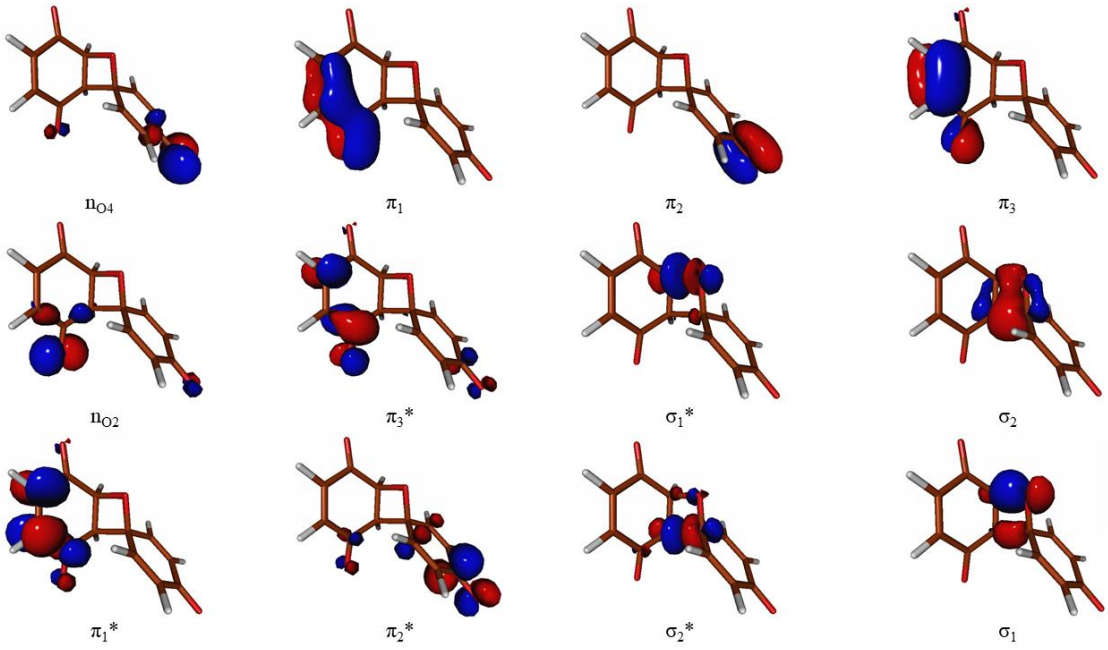

Fig. S5 Natural orbitals of the CASSCF active space of the singlet states at the oxetane structure for BQ-Ox.

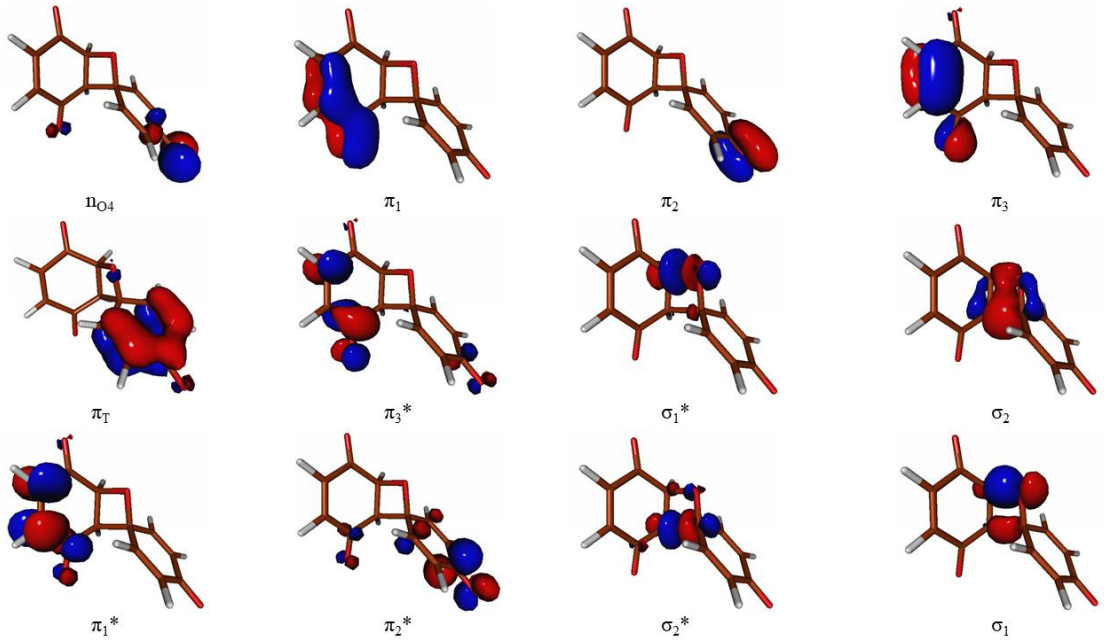

Fig. S6 Natural orbitals of the CASSCF active space of the triplet states at the oxetane structure for BQ-Ox.

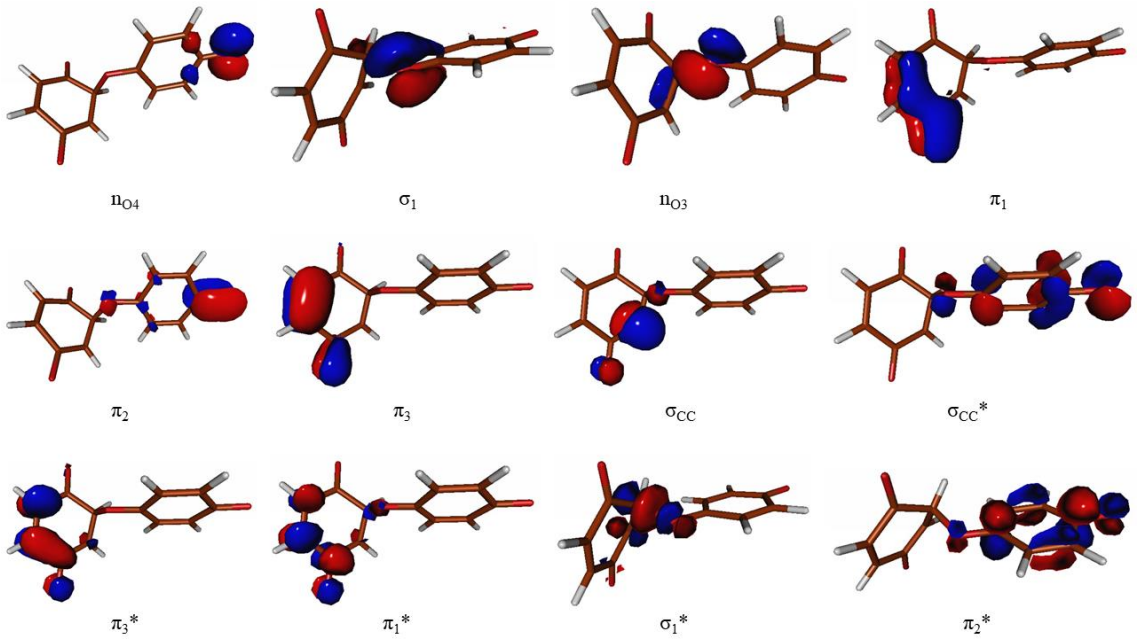

Fig. S7 Natural orbitals of the CASSCF active space of the singlet and triplet states at the diradical structure (^{3}BQ-Ox*) for BQ-Ox.

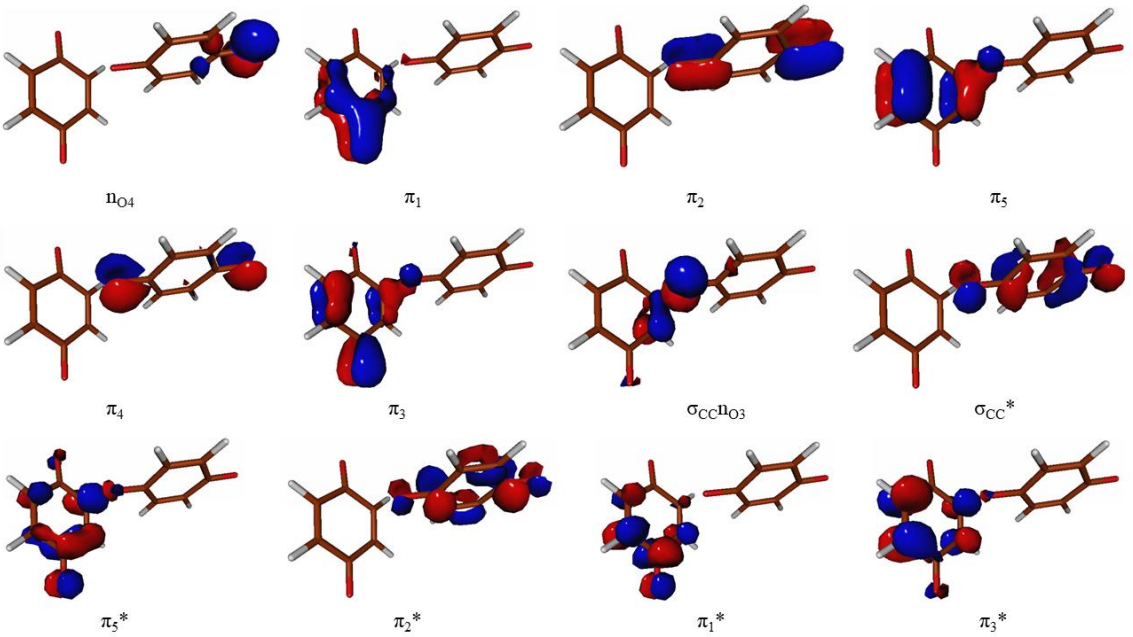

Fig. S8 Natural orbitals of the CASSCF active space of the singlet and triplet states at the transition state structure (TS) for BQ-Ox.

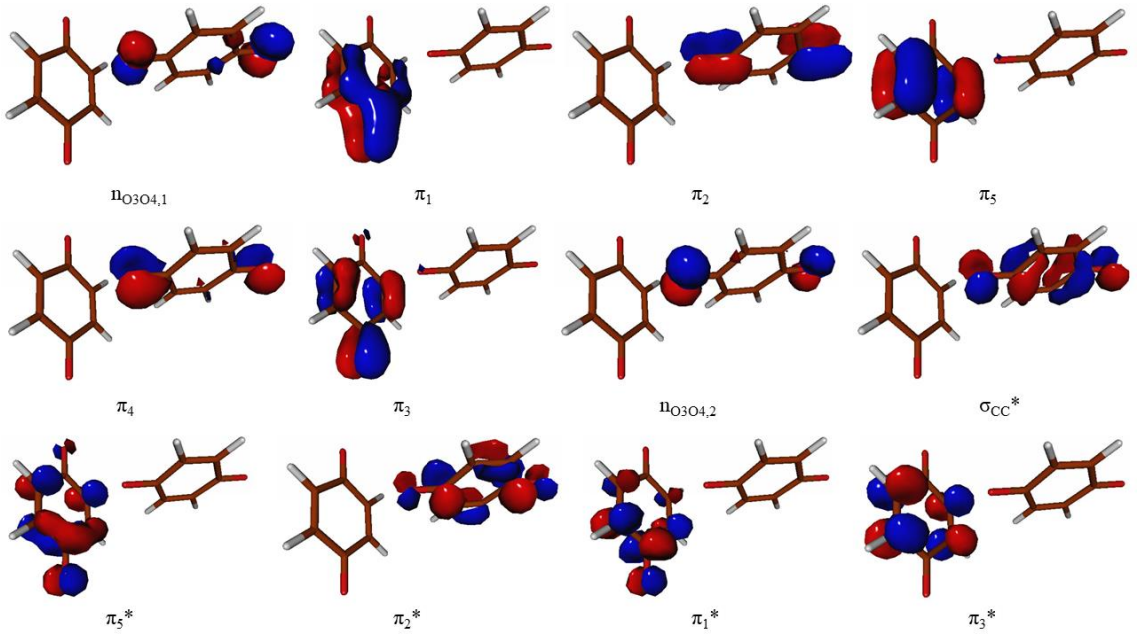

Fig. S9 Natural orbitals of the CASSCF active space of the singlet and triplet states at the excimer structure (^{3}EXC*) for BQ-Ox.

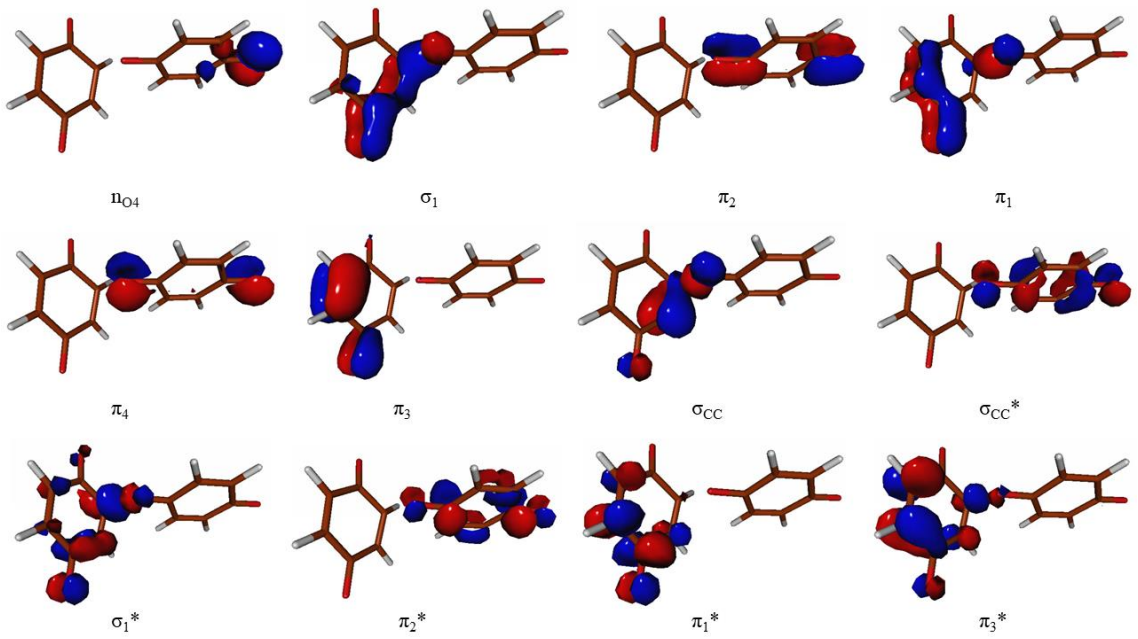

Fig. S10 Natural orbitals of the CASSCF active space of the singlet and triplet states at the crossing point structure (CP) for BQ-Ox.

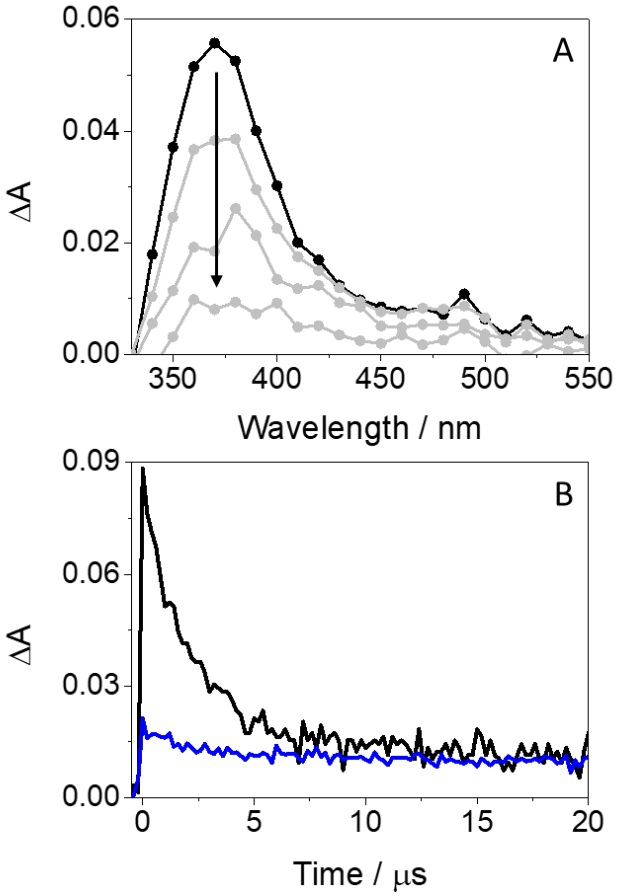

Fig. S11 A) LFP transient absorption spectra for NQ at different times after the laser pulse (0.5, 2, 5 and 20 μs). B) Decay traces for NQ (black) and NQ-Ox (blue) at 370 nm. All measurements were performed in deaerated MeCN at λ_{exc} = 266 nm.

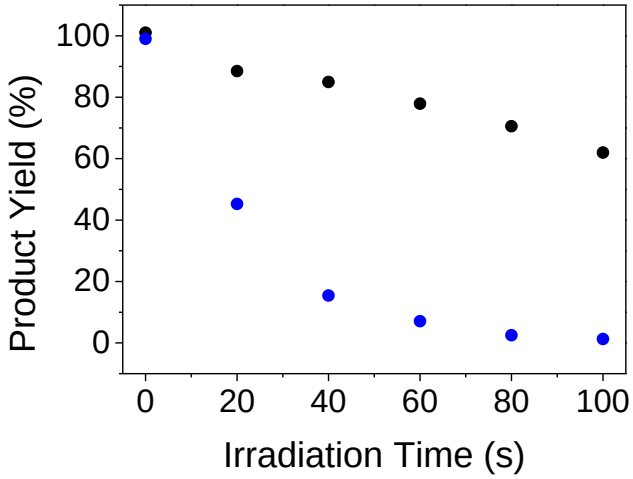

Fig. S12 Degree of photodegradation for NQ (black) and NQ-Ox (blue) upon steady-state irradiation in deaerated MeCN using a multilamp photoreactor emitting at λ_{max} ~ 310 nm.

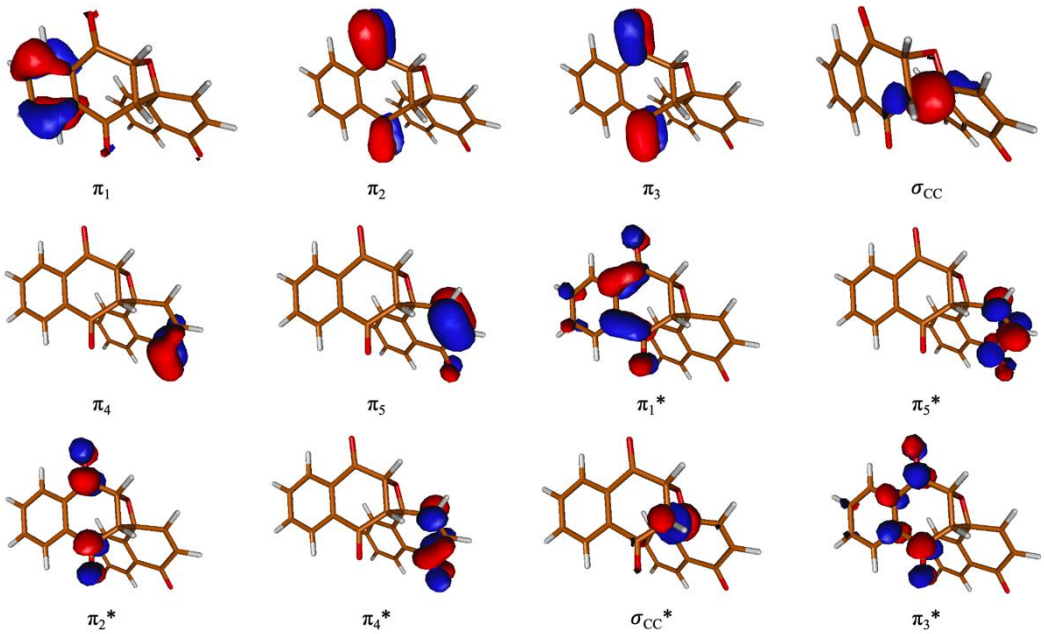

Fig. S13 Natural orbitals of the CASSCF active space of the singlet states at the oxetane structure for NQ-Ox.

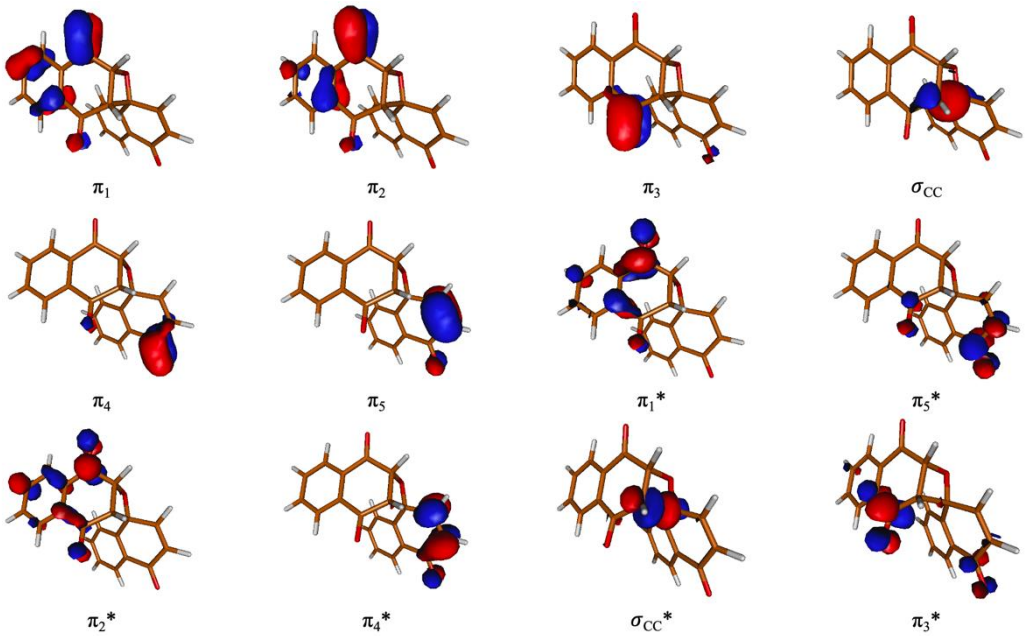

Fig. S14 Natural orbitals of the CASSCF active space of the triplet states at the oxetane structure for NQ-Ox.

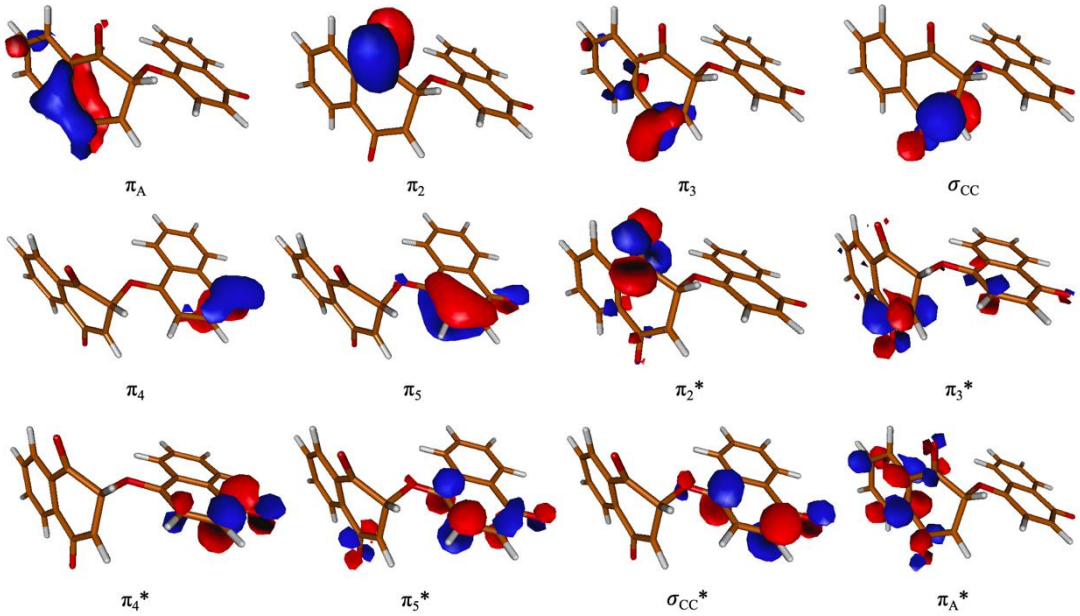

Fig. S15 Natural orbitals of the CASSCF active space of the singlet and triplet states at the diradical structure (^{3}NQ-Ox*) for NQ-Ox.

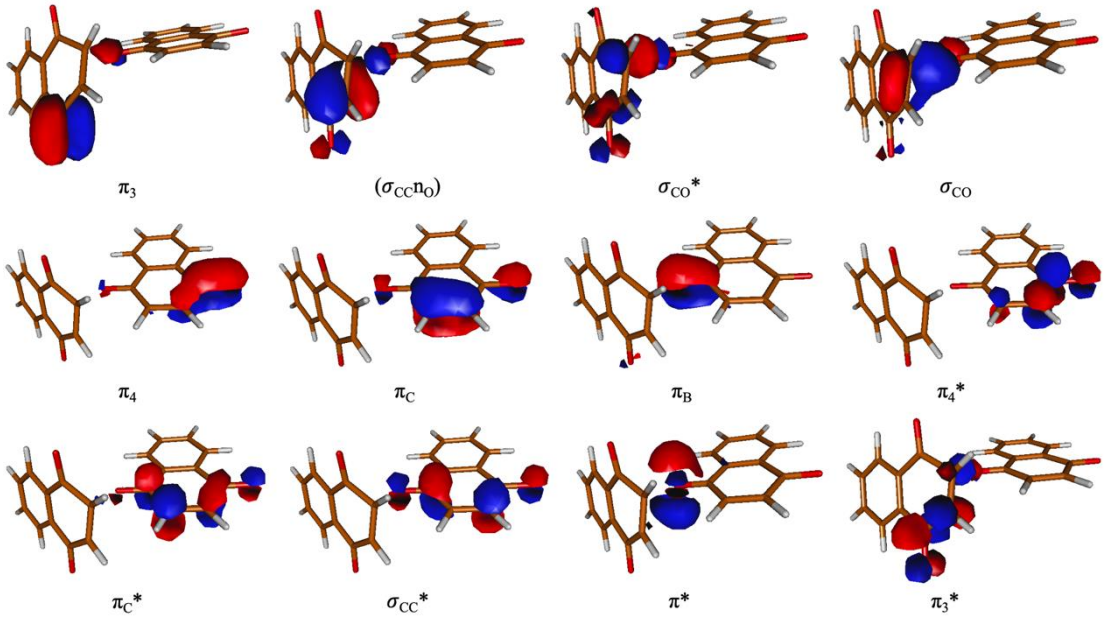

Fig. S16 Natural orbitals of the CASSCF active space of the singlet states at the crossing point structure (CP) for NQ-Ox.

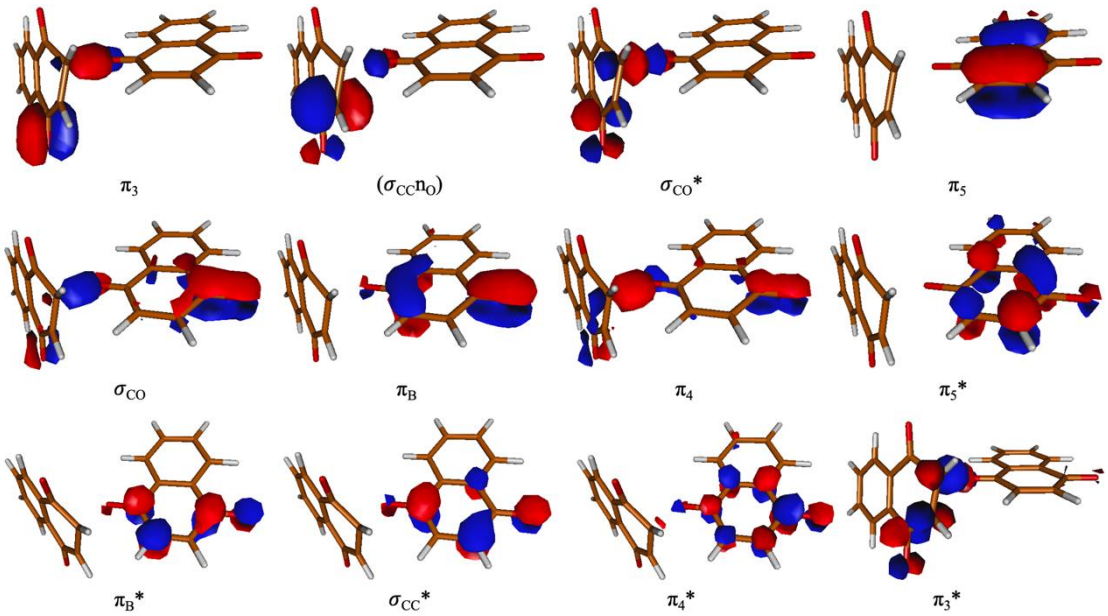

Fig. S17 Natural orbitals of the CASSCF active space of the triplet states at the crossing point structure (CP) for NQ-Ox.

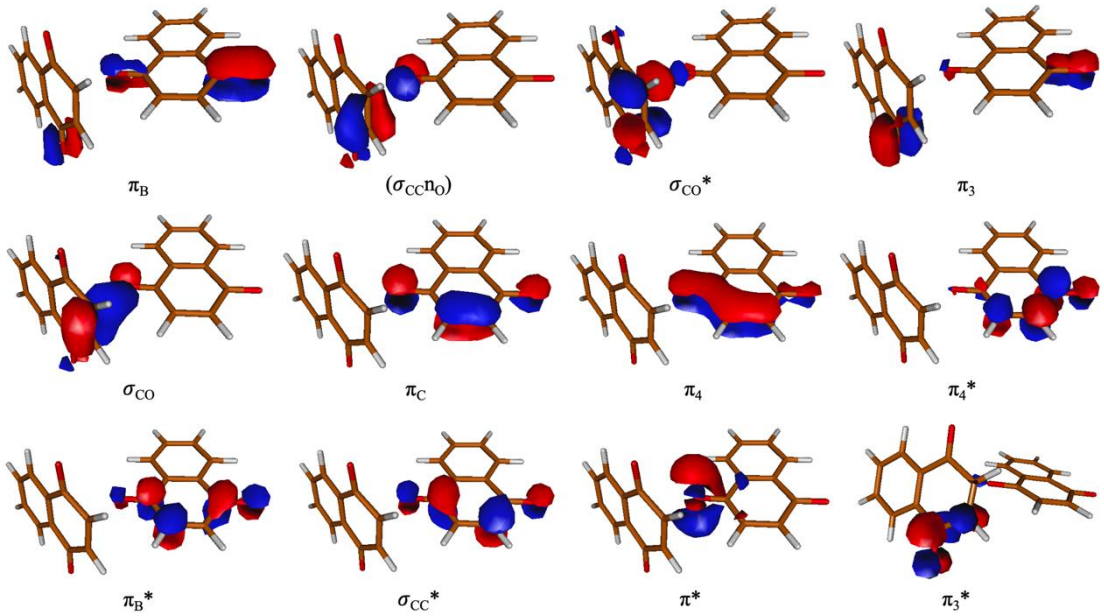

Fig. S18 Natural orbitals of the CASSCF active space of the singlet states at the transition state structure (TS) for NQ-Ox.

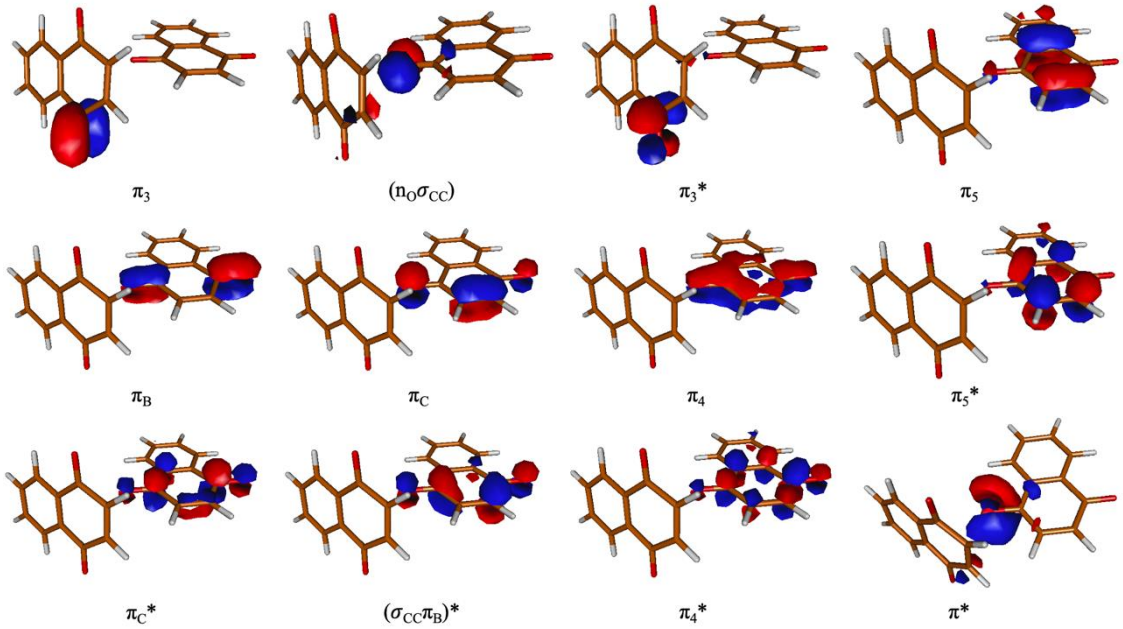

Fig. S19 Natural orbitals of the CASSCF active space of the triplet states at the transition state structure (TS) for NQ-Ox.

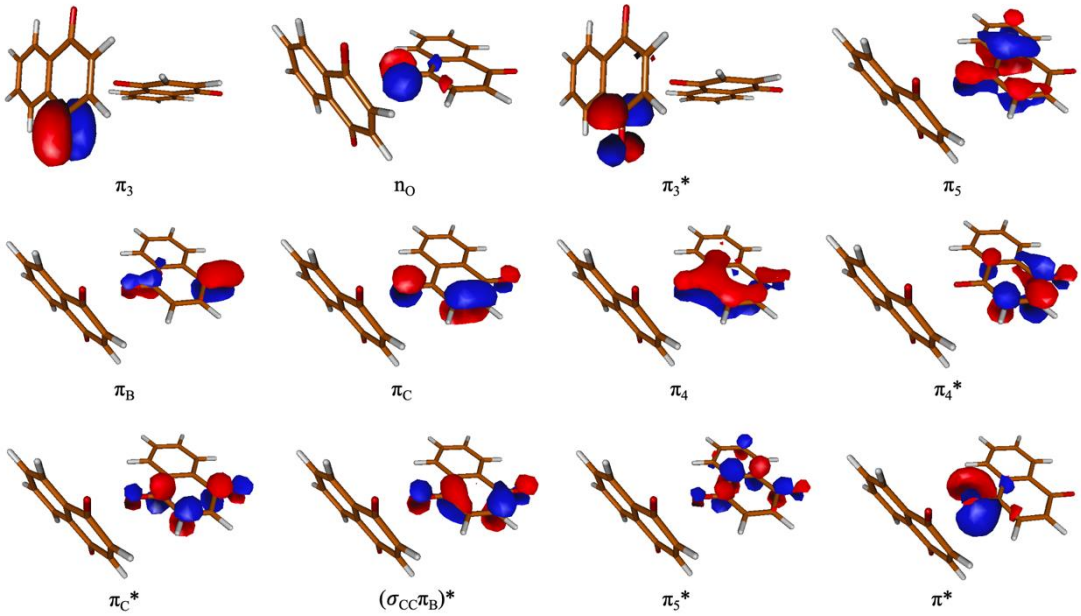

Fig. S20 Natural orbitals of the CASSCF active space of the singlet and triplet states at the excimer structure (^{3}EXC*) for NQ-Ox.

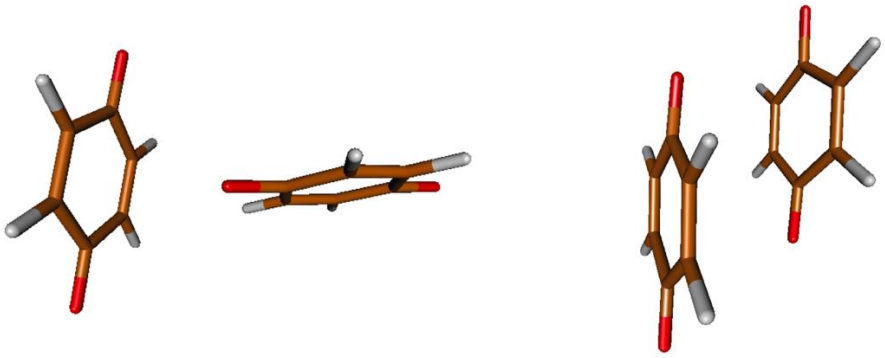

Fig. S21 T-shape and parallel conformations of the ^{3}EXC* for BQ-Ox system.

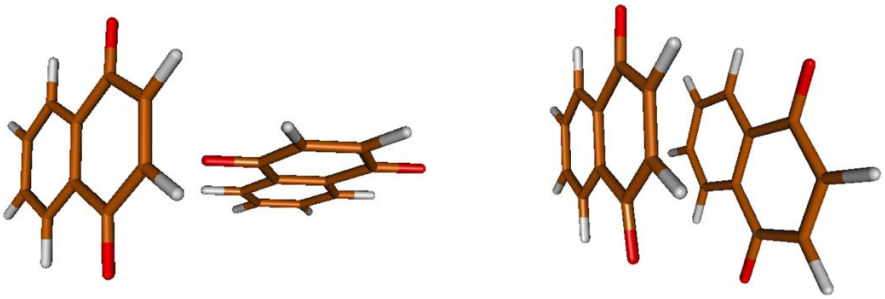

Fig. S22 T-shape and parallel conformations of the ^{3}EXC* for NQ-Ox system.

Table S1 Nature of the states in each relevant geometry for BQ-Ox: energies (E_v^{abs}; in eV), weight of the main configuration state functions in the CASSCF wavefunction (%) and dipole moment (μ; in Debye). See shape of the natural orbitals in Figs. S4 to S9.

Geometry	State	Nature	E_v^{abs}	Weight	μ
BQ-Ox	S_0	cs (HF)[a]	-2.38	78.7	2.00
	S_1	$n_{O1} \rightarrow \pi_2^*$	0.98	67.6	2.08
^{3}BQ-Ox*	S_0	$\sigma_{CC} \rightarrow \sigma_{CC}^*$	-1.38	74.7	3.66
	S_1	$n_{O4} \rightarrow \sigma_{CC}^*/\sigma_{CC} \rightarrow \sigma_{CC}^*$	0.17	81.4	0.97
	T_1	$\sigma_{CC} \rightarrow \sigma_{CC}^*$	-1.39	80.7	3.63
CP	S_0	cs (HF)[a] $\sigma_{CC} \rightarrow \sigma_{CC}^*$	-0.87	53.3 14.7	1.80
	S_1	$\sigma_{CC} \rightarrow \sigma_{CC}^*$ cs (HF)[a] $\pi_4 \rightarrow \sigma_{CC}^*/\sigma_{CC} \rightarrow \sigma_{CC}^*$	-0.80	44.1 17.8 10.5	1.75
	T_1	$\sigma_{CC} \rightarrow \sigma_{CC}^*$ $\pi_4 \rightarrow \sigma_{CC}^*/\sigma_{CC} \rightarrow \sigma_{CC}^*$	-0.80	58.8 12.8	3.97
TS	S_0	cs (HF)[a]	-1.47	71.2	2.07
	S_1	$\sigma_{CC} n_{O3} \rightarrow \sigma_{CC}^*$ $\pi_4 \rightarrow \sigma_{CC}^*/\sigma_{CC} n_{O3} \rightarrow \sigma_{CC}^*$	-0.40	58.0 16.6	2.99
	T_1	$\sigma_{CC} n_{O3} \rightarrow \sigma_{CC}^*$ $\pi_4 \rightarrow \sigma_{CC}^*/\sigma_{CC} n_{O3} \rightarrow \sigma_{CC}^*$	-0.53	59.1 15.2	2.97
^{3}EXC*	S_0	cs (HF)[a]	-2.18	70.9	0.91
	S_1	$n_{O3O4,2} \rightarrow \sigma_{CC}^*$ $n_{O3O4,1} \rightarrow \sigma_{CC}^*$ $\pi_4 \rightarrow \sigma_{CC}^*/n_{O3O4,2} \rightarrow \sigma_{CC}^*$	-0.32	41.7 17.3 123	2.52
	T_1	$n_{O3O4,2} \rightarrow \sigma_{CC}^*$ $\pi_4 \rightarrow \sigma_{CC}^*/n_{O3O4,2} \rightarrow \sigma_{CC}^*$	-0.53	51.8 13.6	2.60

Table S2 Nature of the states in each relevant geometry for NQ-Ox: energies (E_v^{abs}; in eV), weight of the main configuration state functions in the CASSCF wavefunction (%) and dipole moment (μ; in Debye). See shape of the natural orbitals in Figs. S11 to S18.

Geometry	State	Nature	E_v^{abs}	Weight	μ
NQ-Ox	S_0	cs (HF)[a]	-3.79	80.0	3.28
	S_1	$\pi_1 \rightarrow \pi_1^*$	0.03	77.0	5.47
^{3}NQ-Ox*	S_0	$\sigma_{CC} \rightarrow \sigma_{CC}^*$	-2.32	67.7	3.90
	S_1	$\sigma_{CC} \rightarrow \sigma_{CC}^*/\pi_5 \rightarrow \sigma_{CC}^*$ $\sigma_{CC} \rightarrow \pi_5^*$	-0.91	38.9 22.4	3.30
	T_1	$\sigma_{CC} \rightarrow \sigma_{CC}^*$	-2.25	76.1	3.90
CP	S_0	$(\sigma_{CC} n_O) \rightarrow \sigma_{CC}^*$	-1.76	71.1	4.55
	S_1	cs (HF)[a]	-1.75	65.3	5.78
	T_1	$(\sigma_{CC} n_O) \rightarrow \sigma_{CC}^*$	-1.69	77.5	4.81
TS	S_0	cs (HF)[a]	-2.61	75.3	3.16
	S_1	$(\sigma_{CC} n_O) \rightarrow \sigma_{CC}^*$	-1.34	68.1	4.12
	T_1	$(n_O \sigma_{CC}) \rightarrow \sigma_{CC}^*$	-1.18	75.2	3.90
^{3}EXC*	S_0	cs (HF)[a]	-3.48	73.4	1.95
	S_1	$n_O \rightarrow (\sigma_{CC} \pi_B)^*$	-1.28	74.0	3.88
	T_1	$n_O \rightarrow (\sigma_{CC} \pi_B)^*$	-1.40	72.5	3.99

Table S3 DFT and CASPT2 energies (in eV) of the T_1 state of both types of excimers of BQ-Ox and NQ-Ox. The energies are relative to their respective T-shape excimers.

		BQ-ox	**NQ-ox**
$E_{DFT,T1}$	**T-shape**	0.00	0.00
	Parallel	-0.19	-0.28
$E_{CASPT2,T1}$	**T-shape**	0.00	0.00
	Parallel	-0.08	-1.19

REFERENCES

(1) Siegbahn, P. E. M.; Almlöf, J.; Heiberg, A.; Roos, B. O. The Complete Active Space SCF (CASSCF) Method in a Newton–Raphson Formulation with Application to the HNO Molecule. *J. Chem. Phys.* **1981**, *74*, 2384-2396.

(2) Andersson, K.; Malmqvist, P. Å.; Roos, B. O. Second-Order Perturbation Theory with a Complete Active Space Self-Consistent Field Reference Function. *J. Chem. Phys.* **1992**, *96*, 1218-1226.

(3) Frisch, M. J.; Trucks, G. W.; Schlegel, H. B.; Scuseria, G. E.; Robb, M. A.; Cheeseman, J. R.; Scalmani, G.; Barone, V.; Petersson, G. A.; Nakatsuji, H. et al. Gaussian 09, Revision D.01. Gaussian, Inc., Wallingford CT 2009.

(4) Aquilante, F.; Autschbach, J.; Carlson, R. K.; Chibotaru, L. F.; Delcey, M. G.; De Vico, L.; Fdez.-Galván, I.; Ferré, N.; Frutos, L. M.; Gagliardi, L. et al. Molcas 8: New Capabilities for Multiconfigurational Quantum Chemical Calculations across the Periodic Table. *J. Comput. Chem.* **2016**, *37*, 506-541.

(5) Ghigo, G.; Roos, B. O.; Malmqvist, P. Å. A Modified Definition of the Zeroth-Order Hamiltonian in Multiconfigurational Perturbation Theory (CASPT2). *Chem. Phys. Lett.* **2004**, *396*, 142-149.

(6) Forsberg, N.; Malmqvist, P. Å. Multiconfiguration Perturbation Theory with Imaginary Level Shift. *Chem. Phys. Lett.* **1997**, *274*, 196-204.